2021 European Control Conference (ECC)
June 29 - July 2, 2021. Rotterdam, Netherlands

Optimal Active Vibration Isolation Systems for Multiple Noise Sources

S.T. Spanjer, W.B.J. Hakvoort

Abstract

The performance of active vibration isolation systems is limited by several effects, including sensor noise and signal filtering. It is shown in this paper that the joint contribution of those effects to the acceleration of the payload is minimized for a bounded set of parameters of the control system and the mechanics. Notably, a bounded optimal value for the skyhook damper is found. Furthermore, these minimizing parameters are found to be in the feasible design space. In a reference case, the RMS acceleration in the relevant frequency band is found to decrease by a factor of 22 using the proposed optimization method.

1. Introduction

Active vibration isolation systems (AVIS) are widely used to attenuate the effect of floor vibrations on precision payloads. Applications can be found in, for example, wafer steppers [1], gravitational wave detectors [2] and scanning tunnelling microscopes [3]. These systems are developed to circumvent the trade-off in passive systems between the sensitivity to direct and indirect disturbances. That is, direct disturbances act on the sensitive payload, where indirect disturbances work on the sensitive payload through the suspension.

The performance of AVIS depends on the used control method. A traditional example of these control methods is the skyhook damper [4]. The idea of skyhook damping is extended to a skyhook spring [5], and acceleration feedback [6]. These feedback controllers are commonly appended with a feedforward controller to cancel measured indirect disturbances. Recently, promising results are obtained with such a disturbance feedforward controller [7]. This feedforward controller is based on self-tuning, generalized FIR filters whose parameters are adjusted using the filtered error least mean squares approach.

In combination with the control method, the mechanical design and the used actuating and sensing hardware heavily influence the vibration isolation performance [8][9]. Here the used actuating and sensing hardware introduce noise in the system, where the mechanical design acts as analogue filters for the system signals. The sensor noise motivates the use of weak integrators to minimize drift of the system [7]. For the weak integrators as well as the feedback controller, no clear tuning guidelines are currently available.

The control method and its parametrization and the used hardware have an intricate interaction. For example, the effect of the noise of the sensors on the acceleration of the payload is amplified by the controller, whereas the actuator disturbances are attenuated by the controller. This sets the scope for a combined optimization problem, where both the control and the hardware are optimized.

The central research question is therefore: *Does a feasible optimum exist in tuning the mechanical and control parameters for the vibration isolation performance of an active vibration isolation system for a given set of sensing and actuation hardware?* The main contribution of this paper is to show that a feasible limit exists using an optimization approach to dynamic error budgeting [10]. Furthermore, a tuning guideline for weak integrators is introduced. For this, the proposed method is detailed for a real AVIS system.

The remainder of this paper is organized as follows. First, the governing equations of a single degree of freedom AVIS are introduced. Then, the performance limiters are described. This is followed in section 4 by a description of the available sensing and control hardware. The optimization criteria and method are described in section 5. The results are presented in section 6, and discussed in section 7.

2. Active vibration isolation systems

A basic representation of a 1-DoF active vibration isolation system is displayed in figure 1. Here, m_1 is the sensitive payload and x_0 the coordinates of the vibrating floor. The parameters d and k are respectively the suspension damping and stiffness constants and F_a is the actuation force for the active system. The absolute motion is measured at s_0 and s_1. These sensors can either measure absolute position, velocity or acceleration and are subjected to noise. Hereafter, acceleration measurements are considered.

978-94-6384-236-5 ©2021 EUCA

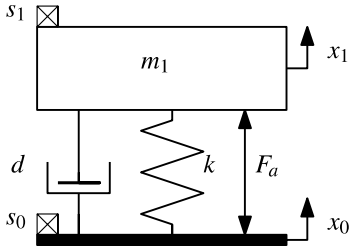

Figure 1: General active vibration isolation system.

The blockscheme of this system is given in figure 2. Here a_0 and a_1 are the acceleration of the floor and the payload respectively. $\hat{a}_0$ and $\hat{a}_1$ are the measured accelerations, which consist of the acceleration and additive measurement noise n_0 and n_1. The primary path and secondary path are given as

$$P_1(s) = \frac{a_1(s)}{a_0(s)} = \frac{1}{ms^2+ds+k}, \tag{2.1}$$

$$P_2(s) = \frac{a_1(s)}{F_a(s)} = \frac{s^2}{ms^2+ds+k}. \tag{2.2}$$

The feedback controller is chosen as a combination of a skyhook spring, skyhook damper and a virtual mass with the corresponding parameters k_x, k_v and k_a respectively, which is described by

$$C_{FB}(s) = \frac{u_{FB}(s)}{\hat{a}_1(s)} = -k_a - \frac{k_v}{s} - \frac{k_x}{s^2}. \tag{2.3}$$

The feedforward controller is chosen such that it perfectly compensates the floor disturbance in the disturbance and noise free case. This can be realised using the following controller, where the exact parameters are assumed to be obtained through adaptation of a generalized FIR filter [7], and is given as

$$C_{FF}(s) = \frac{u_{FF}(s)}{\hat{a}_0(s)} = \frac{d}{s} + \frac{k}{s^2}, \tag{2.4}$$

The transmissibility is the sensitivity of the payload to indirect disturbances and is given as

$$T(s) = \frac{a_1(s)}{a_0(s)} = \frac{P_1(s)+C_{FF}(s)P_2(s)}{1-C_{FB}(s)P_2(s)}. \tag{2.5}$$

The compliance is the sensitivity of the payload to direct disturbances and is given by

$$C(s) = \frac{x_1(s)}{F_d(s)} = \frac{P_2(s)}{1-C_{FB}(s)P_2(s)}, \tag{2.6}$$

where $F_d(s)$ are the direct disturbance forces. In general disturbance force includes the disturbance introduced by the actuators n_a.

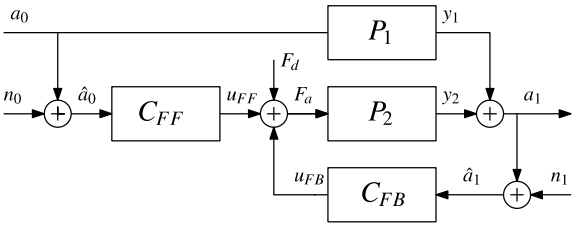

Figure 2: Blockscheme Active vibration isolation system.

The influence of the measurement noises on the acceleration of the payload can be described by the noise sensitivity functions

$$S_0(s) = \frac{a_1(s)}{n_0(s)} = \frac{C_{FF}(s)P_2(s)}{1-C_{FB}(s)P_2(s)}, \tag{2.7}$$

$$S_1(s) = \frac{a_1(s)}{n_1(s)} = \frac{C_{FB}(s)P_2(s)}{1-C_{FB}(s)P_2(s)}, \tag{2.8}$$

Combining the equations introduced here gives the expression for the acceleration of the payload as

$$\begin{aligned} a_1(s) =& T(s)a_0(s) + s^2C(s)F_d(s) \\ &+ S_0(s)n_0(s) + S_1(s)n_1(s). \end{aligned} \tag{2.9}$$

The power spectral density of $a_1(s)$ is

$$\begin{aligned} \bar{S}_{a_1}(s) =& |T(s)|^2\bar{S}_{a_0}(s) + |s^2C(s)|^2\bar{S}_{F_d}(s) \\ &+ |S_0(s)|^2\bar{S}_{n_0}(s) + |S_1(s)|^2\bar{S}_{n_1}(s), \end{aligned} \tag{2.10}$$

where the bar operator indicates a spectrum.
Substituting the feedforward controller of (2.4) into (2.5) yields $T(s) = 0$. An ideal AVIS, without direct disturbances ($F_d(s) = 0$), and no noise ($n_0(s) = n_1(s) = 0$), has therefore $a_1(s) = 0$.

3. Performance limiters

In practice, the performance of an ideal AVIS is limited by some unavoidable adverse effects. These effects include noise and signal conditioning and are presented in this section in more detail. Later, in section 5, these effects are included in optimisation of the system parameters.

3.1. Sensor noise

The shape of the noise profile of absolute motion sensors depends on the sensor principle [9]. Commonly either absolute acceleration or absolute velocity are measured with accelerometers and geophones respectively.

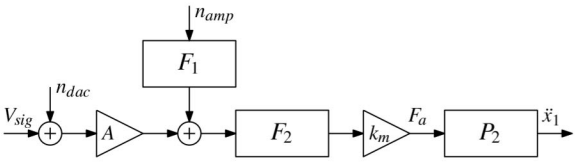

Figure 3: Blockscheme of a general actuator system. The gain A is the amplifier gain in the region of interest. k_m is the force constant.

Accelerometers can use various principles to measure accelerations, of which the most common are piezoelectric and variable capacitance. Variable capacitance accelerometers have a flat noise spectrum, where piezoelectric accelerometers have high low-frequent noise levels, which decrease to a constant level. Geophones have a V-shaped noise spectrum[9]. In general, piezoelectric accelerometers have lower high-frequent noise levels than variable capacitance accelerometers, but specifics depend on the design, material and manufacturing of the sensors.

3.2. Actuator disturbance

The actuators for AVIS need to satisfy requirements in bandwidth, force capacity, stroke and noise levels. Typical actuator types that could satisfy these requirements are piezo electric stacks and voice coil actuators [9]. In general, the actuator force and noise can be described by the blockscheme in figure 3, where the filters F_1 and F_2 depend on the type of actuator and amplifier used.
It can be seen that there are two noise sources in the system, the amplifier noise, and the Digital to Analogue Converter (DAC) noise. The total noise contribution is scaled by the force constant. It therefore is important to match the actuator to the load requirement to minimise the effect thereof.

3.3. Signal conditioning

The sensor signal needs to be filtered to make the signal suitable for the Analogous to Digital Converter (ADC). This filtering serves a couple of purposes. The first is to match the signal amplitude to the measurement range of the AD converters. The second is to make the voltage of the signal proportional to the acceleration. Lastly, the filter serves as an anti-aliasing filter. Due to these filtering steps, the measured acceleration, even in the case of no noise, is only an approximation of the actual acceleration. Since this approximated acceleration signal is used for the construction of the control signals, this limits the performance of the setup. This can be included in the model by replacing $P_2(s)$ by $\tilde{P}_2(s) = K(s)P_2(s)$,

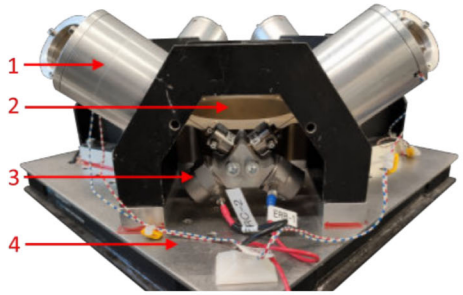

Figure 4: Experimental setup, with; 1) VCM with suspension ; 2) Payload mass; 3) Accelerometer; 4) Floor.

where $K(s)$ describes the signal conditioning filter. This effect shows up in both T and C, which is indicated with $\tilde{T}$ and $\tilde{C}$.

3.4. Weak integrators

The feedback as well as the feedforward controller use the position and the velocity of the payload and floor respectively. These position and velocities need to be reconstructed from the measured signal. The use of pure integrators for estimation of the position and velocity yields drift in these estimates due to the amplification of the noise in the low frequency region.
This drift can be limited by replacing the pure integrators of (2.3) and (2.4) by

$$H_{\alpha,n} = \frac{1 - \left(\frac{\alpha}{s+\alpha}\right)^n}{s} \tag{3.1}$$

which are high pass filtered integrators, also called weak integrators [7]. Here α is the corner frequency and n the order of the weak integrators.

4. Setup

To contextualize the method described in section 5, first the available experimental setup is described. This setup is a Steward platform where the payload mass is connected via wire flexures to six Voice Coil Motors (VCMs), and is shown in figure 4. For a detailed explanation of the experimental setup, the reader is referred to [11, 12]. To quantify the performance limiters as presented in section 3, the following components of the setup are relevant:

- GeePlus VM4032-250 VCM actuators
- Trust automation TA-105 VCM amplifiers (voltage mode)
- Brüel & Kjaer Nexus 2692-0S4 conditioning amplifier

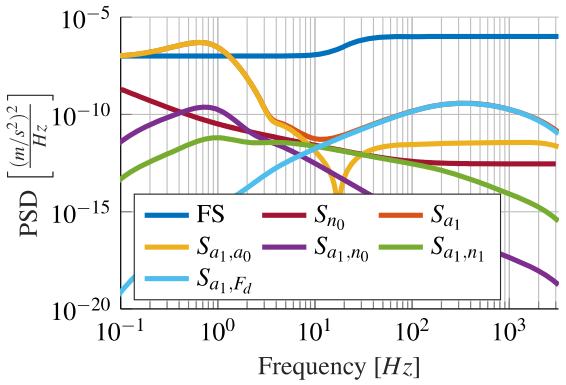

Figure 5: PSD of the original setup. FS: ASML floor spectrum, S_{a_1}: Total a_1, S_{a_1,a_0}: contribution of a_0 on a_1, S_{a_1,n_0}: contribution of n_0 on a_1, S_{a_1,n_1}: contribution of n_1 on a_1, S_{a_1,n_a}: contribution of n_a on a_1

- Endevco 7703A-1000 piezoelectric accelerometers (used to measure floor and payload accelerations)
- dSpace DS2102 DA converter

The system is sampled at $f_s = 6400$ Hz. Here, for simplicity of representation, only the z-direction is considered. The primary and secondary path, see equation 2.1 and 2.2, of this direction are described by $k = 80$ kN/m, $d = 80$ Ns/m and $m = 3.5$ kg.
The accelerometer signals are conditioned by charge amplifiers with built-in are high- and low-pass filters, with cut-off frequencies at 0.1 Hz and 3000 Hz respectively.
The Power Spectral Density (PSD) of the floor is assumed to follow the ASML specification [10].
The reference feedback controller used for this setup is a skyhook damper with $k_v = 3500$. Fifth order weak integrators are used with $\alpha = 2$ Hz [7].
The voltage mode VCM actuators yield a realisation of the filters in figure 3 as $F_1(s) = 1$ and $F_2(s) = \frac{1}{R_c + L_c s}$, with R_c the coil resistance and L_c the coil inductance. From measurements, the sensor spectra are approximated as

$$\bar{S}_{n_0}(s) = \bar{S}_{n_1}(s) = 10^{-10}\frac{2.86\cdot 10^{-3}s^2 + 1.63s + 7.80}{s^2}, \tag{4.1}$$

It is assumed that the direct disturbance spectrum is equal to the actuator noise spectra, which is approximated by[9]

$$\bar{S}_{F_d}(s) = \bar{S}_{n_a}(s) = \frac{1}{(3s + 1.2\cdot 10^4)^2}. \tag{4.2}$$

5. Optimization

The experimental setup has all performance limiters discussed in section 3. They have been separately quantified. This leads to the PSD of the setup with its components as displayed in figure 5 as the starting point of the optimization. It can be seen that the the residual spectrum S_{a_1} is dominated by S_{a_1,a_0} in the low frequency region and S_{a_1,F_d} in the high frequency region. S_{a_1,a_0} is caused by a non-zero transmissibility as a result of the weak integrators and the signal conditioning.

5.1. Optimization criteria

The following minimization problem is solved for this system

$$\begin{aligned} J &= \underset{\boldsymbol{\theta}\in\boldsymbol{\Theta}}{\operatorname{argmin}} \left\{ \int_{f_1}^{f_2} \bar{S}_{a_1}(\boldsymbol{\theta}, j2\pi f)\, df \right. \\ &\qquad \left. + \sigma \max(0, P(\boldsymbol{\theta}) - \gamma) \right\} \\ &= \underset{\boldsymbol{\theta}\in\boldsymbol{\Theta}}{\operatorname{argmin}} \{V_1(\boldsymbol{\theta}) + V_2(\boldsymbol{\theta})\} \end{aligned} \tag{5.1}$$

in which $\boldsymbol{\Theta}$ is the feasible parameter space. $V_1(\boldsymbol{\theta}) + V_2(\boldsymbol{\theta})$ is the cost function, where $V_2(\boldsymbol{\theta})$ penalizes the cost function when the drift power P, see equation 5.3, exceeds the bound γ. σ is the penalty constant. f_1 and f_2 define the integrand bounds which corresponds to the bandwidth of the optimization. Here, $f_1 = 0.1$ Hz and $f_2 = 1000$ Hz.
The vector $\boldsymbol{\theta}$ contains the optimization parameters and is defined as $\boldsymbol{\theta} = [k, \alpha, k_x, k_v, k_a]^T$, which are the mechanical suspension stiffness, corner frequency of the weak integrators, skyhook spring stiffness, skyhook damper constant and virtual mass respectively.

5.2. Drift limiting

As mentioned in section 3.4, the weak integrators are used to limit the drift of the setup. There are practical limits to the allowable drift in the setup. These limitations stem from the allowable suspension and actuator stroke. For the actuators, drift in the position and the velocity will cause the output of the actuator to saturate.
The drift is a function of the different noise contributions and the system transfer functions. The power spectral density of this drift can be expressed as

$$\begin{aligned} \bar{S}_e(s) = \frac{\bar{S}_{a_1}(s) - \bar{S}_{a_0}(s)}{s^2} &= \frac{1}{s^2}\left\{ |\tilde{T}(s) - 1|^2 \bar{S}_{a_0}(s) \right. \\ &\left. + |s^2\tilde{C}(s)|^2 \bar{S}_{n_a}(s) + |S_0(s)|^2 \bar{S}_{n_0}(s) + |S_1(s)|^2 \bar{S}_{n_1}(s) \right\}, \end{aligned} \tag{5.2}$$

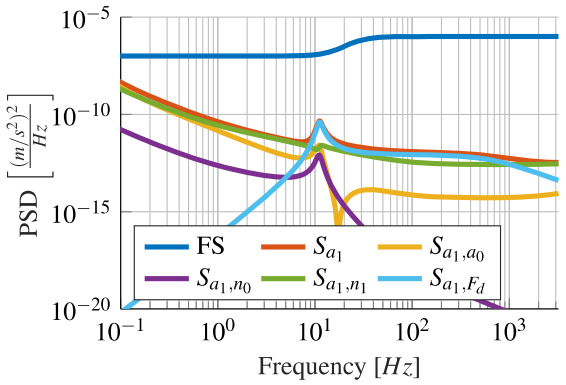

Figure 6: PSD of the optimized setup. See figure 5 for the labels

where the drift power is

$$P = \int_{f_{e_1}}^{f_{e_2}} \bar{S}_e(j2\pi f)\, df. \tag{5.3}$$

The integrand is bounded by f_{e_1} and f_{e_2} and are $1 \cdot 10^{-5}$ Hz and $1 \cdot 10^{3}$ Hz respectively.

5.3. Optimization method

The cost function is optimized by a two-stage optimization procedure. The first step is to explore the solution space using a grid search where the parameter space is sampled with a logarithmic Latin hypercube. The absolute minima of this exploratory search is refined using a gradient descent method. The integrals of (5.1) and (5.2) are numerically approximated using an adaptive quadrature with a relative tolerance of $1 \cdot 10^{-10}$.

6. Results

The optimization problem is solved for two cases. The first is optimizing all available parameters. For the second case k_a and k_x are fixed to zero, this results in a pure skyhook damper feedback controller, which is commonly used. The results of these optimisations and the original settings [7] are given in table 1. Here also the RMS acceleration is given. This RMS value is determined as $\text{RMS}_{a_1} = \sqrt{V_1(\boldsymbol{\theta})}$. It can be seen that only using skyhook improves the RMS acceleration with a factor of 3.8 w.r.t. the original settings. This is mainly due to a lower weak-integrator corner frequency and a higher skyhook damping. Furthermore, adding a skyhook spring and virtual mass yields a predicted improvement in the RMS acceleration by a factor of 21.5.

The PSD of the optimized setup is given in figure 6. It can be seen that the components of the PSD are

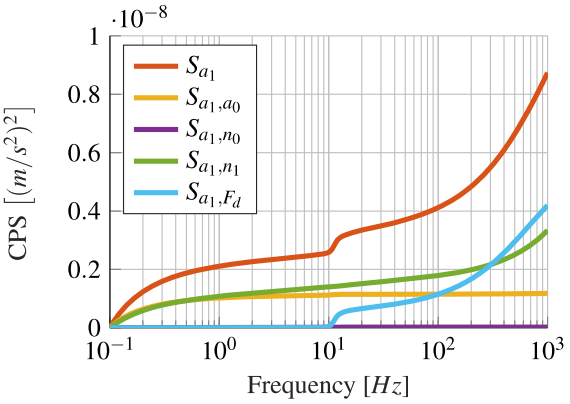

Figure 7: Cumulative Power Spectrum in the optimization bandwidth for the fully optimized setup. See figure 5 for the labels

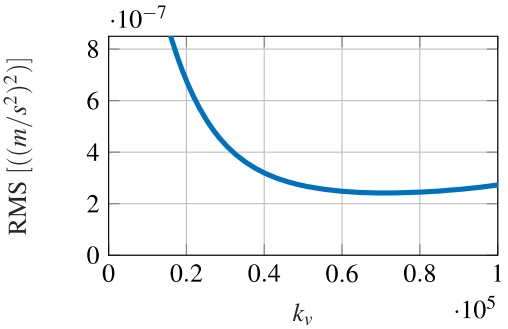

Figure 8: RMS acceleration as a function of the skyhook damper for the skyhook damper optimized case.

balanced when compared to figure 5. The cumulative PSD of this optimized setup is given in figure 7. The floor sensor only marginally contributes to the overall acceleration, furthermore there is a clear balance between the different contributions.

In figure 8 the RMS of the acceleration is given as a function of the skyhook damper using the original values for α and k. Here clearly a feasible minimum can be seen. The same holds for the fully optimized case, where also the minimum is found to exist and is within the feasible space.

7. Discussion

It can be seen in figure 6, that the optimal solution balances the different contributions to the payload acceleration. Below the 10Hz, this balance is dominated by the indirect disturbances ($S_{a_1 a_0}$), and the payload sensor noise ($S_{a_1 n_1}$). For frequencies higher than 10Hz, the direct disturbance ($S_{a_1 F_d}$) is balanced with the payload sensor noise ($S_{a_1 n_1}$).

The balance of $S_{a_1 F_d}$ and $S_{a_1 n_1}$ is governed by the feedback controller and is the reason that the optimal

	k [N/m]	α [Hz]	k_x	k_v	k_a	RMS $[m/s^2]$
Original	$8 \cdot 10^4$	2	0	3500	0	$2.0 \cdot 10^{-3}$
Skyhook damper optimized	$8.1 \cdot 10^4$	$2.0 \cdot 10^{-2}$	0	$7.4 \cdot 10^4$	0	$5.3 \cdot 10^{-4}$
Fully optimized	$3.4 \cdot 10^4$	$2.0 \cdot 10^{-2}$	$3.7 \cdot 10^5$	$7.8 \cdot 10^2$	$8.0 \cdot 10^1$	$9.3 \cdot 10^{-5}$

Table 1: Original and optimized parameters.

feedback tuning is bounded.
The balance between $S_{a_1 a_0}$ and $S_{a_1 n_1}$ is obtained by a decrease in transmissibility at low-frequencies. This is caused by the decreased corner-frequency of the weak-integrators. The optimal value for α is equal for both optimization cases and corresponds to the intersection of the sensor noise spectrum and the ASML floor spectrum, see figure 5. This intersection point does not violate the drift specifications. Therefore, it is suggested that the tuning of α should be chosen at this intersection point.
Furthermore, the obtained balance can be used to identify the bottleneck of the system. For this experimental setup for example, the first candidate to upgrade is the payload accelerometer, since the noise of this sensor is dominant for most of the frequency range.
The system is modelled without parasitic eigenfrequencies and discretization effects which could limit the parameters of the feedback controller. These effects can be included in the system description in section 2, and as a stability constraint in the optimization.

8. Conclusion and future work

A method is proposed to concurrently optimize both controller and physical parameters. Application of this optimization based dynamic error budgeting method yields a predicted improvement in RMS acceleration of a factor of 21.5. Furthermore, a bounded optimal value for the skyhook damper is found. The addition of a skyhook spring and virtual mass also results in a bounded optimum. Furthermore, the optimization did result in a tuning guideline for the weak integrators.
A natural progression of this work is to include the stability constraints to the optimization, as well as extending the design freedom of the controller through H_2 optimization. Furthermore, experimental validation of the results are a valuable addition to the proposed method.

Acknowlegdments

The authors would like to thank R.de Boer for initiating this work in his BSc. thesis, and MI-partners and PM for the financial support.

References

[1] R.-H. M. Schmidt, "Ultra-precision engineering in lithographic exposure equipment for the semiconductor industry," *Philosophical Transactions of the Royal Society A: Mathematical, Physical and Engineering Sciences*, vol. 370, no. 1973, pp. 3950–3972, 2012.
[2] F. Matichard, B. Lantz, K. Mason, R. Mittleman, B. Abbott, S. Abbott, E. Allwine, S. Barnum, J. Birch, S. Biscans *et al.*, "Advanced ligo two-stage twelve-axis vibration isolation and positioning platform. part 1: Design and production overview," *Precision Engineering*, vol. 40, pp. 273–286, 2015.
[3] K.-J. Lan, J.-Y. Yen, and J. A. Kramar, "Sliding mode control for active vibration isolation of a long range scanning tunneling microscope," *Review of scientific instruments*, vol. 75, no. 11, pp. 4367–4373, 2004.
[4] D. Karnopp, M. J. Crosby, and R. Harwood, "Vibration control using semi-active force generators," 1974.
[5] J. Fanson and T. K. Caughey, "Positive position feedback control for large space structures," *AIAA journal*, vol. 28, no. 4, pp. 717–724, 1990.
[6] A. Preumont, A. Francois, F. Bossens, and A. Abu-Hanieh, "Force feedback versus acceleration feedback in active vibration isolation," *Journal of sound and vibration*, vol. 257, no. 4, pp. 605–613, 2002.
[7] M. Beijen, M. Heertjes, J. Van Dijk, and W. Hakvoort, "Self-tuning mimo disturbance feedforward control for active hard-mounted vibration isolators," *Control engineering practice*, vol. 72, pp. 90–103, 2018.
[8] A. Preumont, M. Horodinca, I. Romanescu, B. De Marneffe, M. Avraam, A. Deraemaeker, F. Bossens, and A. A. Hanieh, "A six-axis single-stage active vibration isolator based on stewart platform," *Journal of sound and vibration*, vol. 300, no. 3-5, pp. 644–661, 2007.
[9] G. W. van der Poel, *An exploration of active hard mount vibration isolation for precision equipment*. Ph. D. thesis, University of Twente, Enschede, The Netherlands, 2010.
[10] R. M. Schmidt, G. Schitter, and A. Rankers, *The Design of High Performance Mechatronics-: High-Tech Functionality by Multidisciplinary System Integration*. Ios Press, 2020.
[11] D. Tjepkema, "Active hard mount vibration isolation for precision equipment," 2012.
[12] L. van de Ridder, W. Hakvoort, D. M. Brouwer, J. van Dijk, J. C. Lötters, and A. de Boer, "Coriolis mass-flow meter with integrated multi-dof active vibration isolation," *Mechatronics*, vol. 36, pp. 167–179, 2016.